Article:
Sengokmen-Ozsoz, N., Boston, R., Dean, J.S. et al. (2025) Fabrication of hierarchically porous carbon lattices derived from 3D-printed polymerized high internal phase emulsions. Carbon, 234. 119933. ISSN: 0008-6223

https://doi.org/10.1016/j.carbon.2024.119933

Carbon 234 (2025) 119933

Contents lists available at ScienceDirect

Carbon

journal homepage: www.elsevier.com/locate/carbon

Fabrication of hierarchically porous carbon lattices derived from 3D-Printed polymerized high internal phase emulsions

Nihan Sengokmen-Ozsoz [a,b,c], Rebecca Boston [c], Julian S. Dean [c], Cornelia Rodenburg [c], Frederik Claeyssens [b,c,*]

[a] Department of Materials Science and Engineering, Gebze Technical University, Gebze, Kocaeli, 41400, Turkey
[b] Kroto Research Institute, School of Chemical, Materials and Biological Engineering, The University of Sheffield, Sheffield, S3 7HQ, United Kingdom
[c] School of Chemical, Materials and Biological Engineering, Sir Robert Hadfield Building, The University of Sheffield, Mappin Street, Sheffield, S1 3JD, United Kingdom

ARTICLE INFO

Keywords:
Vat photopolymerization
Emulsion templating
polyHIPEs
Porous carbon
carboHIPE
Lattice

ABSTRACT

Porous carbons have drawn significant scientific interest, mainly due to carbon's chemical stability, affordability, and exceptional surface area. These materials find applications in diverse areas such as energy storage devices, water contaminant adsorption, and gas separation. Emulsion templating followed by pyrolysis is a promising method to fabricate hierarchically porous carbon materials with interconnected pores at various scales and high surface areas. Combining this technique with additive manufacturing, in particular vat photopolymerization, offers opportunities for creating intricate, inherently porous materials with hierarchical porosity, including carbon lattice structures.

Using high internal phase emulsions (HIPEs) as resin for vat photopolymerization allows for the fabrication of templates with multiscale (10 μm and 100 μm) porosity— which is challenging for 3D printing.

This study investigated the use of inherently porous 3D-printed polymerized **H**igh **I**nternal **P**hase **E**mulsion (polyHIPE) lattice structures to fabricate hierarchically porous carbonized **H**igh **I**nternal **P**hase **E**mulsion (carboHIPE) lattices. Surfactant-stabilized water-in-oil emulsions, based on 2-ethylhexyl-acrylate and isobornyl-acrylate as a 3D printing resin, were used to produce polyHIPE lattices with three distinct porosities (80 %, 85 %, and 87.5 %). The inherently porous lattice-shaped polyHIPEs were pyrolyzed at various temperatures (500 °C, 600 °C, 700 °C, and 800 °C) to fabricate carboHIPE lattices.

Overall, this study introduced a novel method for fabricating hierarchically porous carboHIPE lattice structures using a combination of emulsion templating and additive manufacturing, followed by pyrolysis. This approach highlighted the challenge of directly achieving micro-sizes in the final shape but also demonstrated that the shrinkage during pyrolysis could be beneficial for creating hierarchically porous microlattice carbon structures.

1. Introduction

In recent decades, there has been growing interest in the production of porous polymer structures due to their versatility in design and relatively cost-effective manufacturing process [1–3]. The research focuses on porous polymers and creating polymers with adjustable physical properties, well-defined porosities ranging from micrometer to millimeter sizes, and high surface areas. This has opened up various potential applications, including filter materials, catalyst supports, and scaffold materials for tissue engineering and 3D cell culture [1]. Porous polymers can also serve as templates for manufacturing porous metals, ceramics, carbons, and composites. Moreover, by mimicking the configurations found in naturally occurring porous materials, diverse porous arrangements have been created, including foams, honeycombs, and lattices [4–7].

Porous materials possessing substantial surface areas, particularly within the category of porous carbons, have attracted considerable scientific attention [8]. This interest primarily stems from carbon's chemical stability and affordability. Porous carbons can be used in various applications, including their use as electrodes in energy storage

* Corresponding author. Kroto Research Institute, School of Chemical, Materials and Biological Engineering, The University of Sheffield, Sheffield, S3 7HQ, United Kingdom.
E-mail address: f.claeyssens@sheffield.ac.uk (F. Claeyssens).

https://doi.org/10.1016/j.carbon.2024.119933
Received 30 September 2024; Received in revised form 2 December 2024; Accepted 18 December 2024
Available online 19 December 2024

devices like lithium-ion batteries [9] and supercapacitors [10], as adsorbents for water contaminants [11,12], and materials for gas separation [13].

Numerous conventional methods have been devised for creating carbon-based materials, including carbonization and activation processes [14,15]. Carbonization involves high-temperature decomposition of carbon precursors under inert conditions, leading to porous carbon materials [16,17]. Various techniques, including pyrolysis [18], hydrothermal carbonization (HTC) [19], chemical vapor deposition (CVD) [20], ball milling [21], and arc discharge [22], are employed, influencing the resulting structure, morphology, and composition of the porous carbons. Activation processes, chemical and physical, play a vital role in restoring porosity, with chemical activation introducing nano porous carbon structures [23].

Nonetheless, conventional techniques produce porous carbons with restricted adjustability in terms of porous structure, pore sizes. In contrast, emulsion-based approaches, such as emulsion templating, emulsion polymerization/microencapsulation, and emulsion freeze drying, are emerging as promising methods to fabricate hierarchically porous carbon materials with interconnected pores at various scales and high surface areas [14,24].

Emulsion templating is a manufacturing technique used to create porous interconnected polymeric materials, with a particular focus on polymerized high internal phase emulsions, commonly referred to as PolyHIPEs [1,2]. In this process, two immiscible liquids, one forming the continuous (organic) phase and the other the internal (droplet) phase, are mixed and stabilized through the addition of surfactants [25,26] or colloidal particles [27–29]. An emulsion is classified as a high internal phase emulsion (HIPE) when the internal phase is more than 74 % of the total volume, which represents the maximum volume that can be occupied by uniform spheres [30]. The production of PolyHIPEs involves further polymerization of the continuous phase and subsequent removal of the internal phase.

Emulsion-templated polymers exhibit significant potential as precursors for customizable carbon foams [31–33]. They allow for precise control over the emulsion droplets used as templates, thereby enhancing control over structural characteristics. Additionally, they maintain a monolithic structure and have the advantage of originating from liquid precursors, enabling them to be shaped into virtually any form. By subjecting polyHIPEs to carbonization, emulsion-templated carbon foams, referred to as carboHIPEs, can be created [33–35].

Various carbon precursors derived from polyHIPEs have been reported, including lignin [36], polyacrylonitrile [37], resorcinol-formaldehyde [38], and tannins [39]. So far, extensive investigations have focused on styrene-co-divinylbenzene (ST-co-DVB) copolymers and DVB-based polymers for creating porous carbons through emulsion templating followed by pyrolysis [8,32,34,35,40–46]. Nonetheless, to fabricate carboHIPEs from ST-co-DVB/DVB-based polyHIPEs, additional stabilization is required due to their relatively limited thermal stability [47]. In addition, dicyclopentadiene (DCPD)-based polyHIPEs have recently been explored as a promising precursor for producing carboHIPEs, which exhibit unique properties and have shown potential in advanced applications, such as Li–O_2 [48] and Li–S [49] batteries.

Broadening the scope of porous materials can be achieved through the fabrication of inherently porous complex structures using polyHIPEs to achieve hierarchical pore constructs. The combination of additive manufacturing and emulsion templating opens up opportunities for creating inherently porous materials in intricate forms with hierarchical porosity. Among various additive manufacturing (AM) techniques, vat photopolymerization stands out for its ability to directly fabricate 3D intricate structures from design files with minimal effort. Recently, a polymer resin with inherent porosity through emulsion templating was developed in our group [50–52], and we have reported its use as a resin for vat photopolymerization based commercial 3D printers [53]. Additionally, in our previous study, we successfully demonstrated the creation of intricate hierarchical porous architectural designs using HIPEs through additive manufacturing [54]. This approach enables the utilization of PolyHIPEs as templates for creating inherently porous carbon lattice structures.

In this study, we employed a surfactant-stabilized water-in-oil emulsion, based on 2-ethylhexyl-acrylate and isobornyl-acrylate, as a 3D printing resin. This resin was utilized to produce polyHIPE lattices with three distinct porosities (80 %, 85 %, and 87.5 %) via vat photopolymerization-based 3D printing using an Elegoo Saturn 2 8 K 3D printer. Following this, inherently porous lattice-shaped polyHIPEs were subjected to pyrolysis at various processing temperatures (500 °C, 600 °C, 700 °C, and 800 °C). The macrostructure of the bare polyHIPEs remained intact after pyrolysis. Subsequently, we conducted a detailed characterization of the resulting carboHIPEs derived from the acrylate-based polyHIPEs. Finally, the mechanical properties of the carboHIPE lattices with different porosities were assessed.

2. Experimental

2.1. Materials

2-ethylhexyl acrylate (EHA), isobornyl acrylate (IBOA), trimethylolpropane triacrylate (TMPTA), a photoinitiator; diphenyl (2,4,6- trimethyl benzoyl)-phosphine oxide/2-hydroxy-2-methyl propiophenone (blend), beta carotene (synthetic, ≥93 % (UV), powder), and tartrazine (dye content ≥85 %) were all purchased from Sigma Aldrich. The surfactant Hypermer B246–SO-M was received from Croda.

2.2. Methods

2.2.1. Preparation of high internal phase emulsions

The combination of EHA/IBOA/TMPTA monomers was first used in 2006 by Pierre et al. [55]. A continuous organic phase was prepared by mixing 39.70 wt% of 2-ethylhexyl acrylate (EHA), 39.70 wt% of isobornyl acrylate (IBOA), 15.90 wt% of trimethylolpropane triacrylate (TMPTA) as the crosslinker, and 4.70 wt% of Hypermer B246–SO-M as the surfactant (Table S1). To dissolve the surfactant completely, the mixture was heated to 50 °C. Beta-carotene and tartrazine, previously reported in our prior research, were incorporated at concentrations of 0.02 wt% and 0.06 wt%, respectively, within the continuous organic phase, as light-absorbers [54]. The photoinitiator was then added at 5 wt % into the continuous phase. To create an emulsion, distilled water (dH_2O) was added drop by drop while stirring the mixture at 300 rpm using a SciQuip-Pro 40 stirrer. HIPEs were prepared using 80 vol%, 85 vol%, and 87.5 vol% of dH_2O to create polyHIPEs with 3 different porosities.

2.2.2. 3D printing of polyHIPE lattices

PolyHIPE structures were manufactured using a commercial 3D printer, the Elegoo Saturn 2 8 K, which employs digital light processing technology. This 3D printer is equipped with an 8 K monochrome LCD screen boasting a resolution of 7680 × 4320 pixels and a XY resolution of 28.5 μm [56]. It is further enhanced with a chip-on-board lens combined with integrated UV LED lights and a Fresnel lens, which collaboratively provide a consistent 405 nm light source for printing. The Fresnel collimating light source comprises 48 highly integrated UV LED lights that, in conjunction with the FCL system and Fresnel lens, emit a uniform 405 nm wavelength light, resulting in exceptional printing precision and a smoother surface finish.

The lattice structure consisting of tetrahedral octahedral vertex centroid unit cell configuration (to be mentioned as “lattice structure” or “lattice” in the text) was obtained from thingiverse.com [57]. Autodesk Fusion 360 was used to add a base to the lattice structure (Fig. S1). The 3D design was formatted as.stl file and then sliced using CHITUBOX Basic.

24 mm × 24 mm × 20 mm lattice structures including 25 mm × 25

mm × 3 mm of the base were 3D printed with a layer thickness of 60 μm (Fig. 1B–D). The pore sizes of the 3D-printed 80 %, 85 %, and 87.5 % porous polyHIPEs were 21.20 ± 6.11 μm, 26.26 ± 7.33 μm, and 34.63 ± 13.15 μm, respectively (Fig. S3). The 3D printing parameters including exposure time, bottom layer count, and bottom exposure time etc. were presented in Table S2. It is essential for the initial layers to have a longer exposure time compared to the standard exposure time to ensure proper adhesion of the structures to the printing platform. The entire 3D printing process took approximately 3 h to produce 15 lattices in a single batch.

Following the completion of the 3D printing process, the printed structures were rinsed with methanol to remove any materials eluting from the polyHIPE, such as uncured resin. They were then placed in an oven at 65 °C for a 24-h period for drying.

2.2.3. Carbonization of 3D printed polyHIPE lattices

The PolyHIPE lattices to produce hierarchically porous carboHIPE lattices were pyrolyzed under N_2 atmosphere in a high-temperature oven (Elite tube furnace, Elite Furnaces, UK). 4 different processing temperatures, 500 °C, 600 °C, 700 °C, and 800 °C were used to investigate the carbonization mechanism of PolyHIPEs under various temperatures as determined by their TGA analysis, where the decomposition initiates at 500 °C (Fig. S2). The temperature was raised to the processing temperature at a rate of 5 °C/min, and it was held at that temperature for a period of 2 h.

2.3. Characterization

2.3.1. Mercury intrusion Porosimetry

The degree of porosity and the bulk densities of the polyHIPE and carboHIPE lattices were measured using a mercury intrusion porosimeter (AutoPore V, Micrometrics). The highest applied pressure and the contact angle of mercury were 60000 psi (414 MPa) and 130°, respectively.

2.3.2. Scanning electron microscopy (SEM)

An FEI Inspect F scanning electron microscope (SEM) was employed to visualize both the macrostructure and microstructure of carboHIPEs. Imaging was performed with an accelerating voltage of 5 kV. Pore sizes were quantified using ImageJ. 70 pores measured from each category and the images used for pore size measurements were presented in supporting information (Figs. S3, S5, S7 and S9). To address potential underestimation of pore diameters resulting from uneven sectioning, a statistical correction factor ($2/\sqrt{3}$) was applied to the pore size measurements [58].

2.3.3. Raman spectroscopy

The carboHIPE samples were analyzed by Raman spectroscopy (Renishaw InVia) using a 20 mW, 514.5 nm laser and a 50 × objective, between Raman shifts of 100 cm^{-1} and 4000 cm^{-1}. The exposure time was 10 s, with 8 accumulations collected per sample. Baseline correction

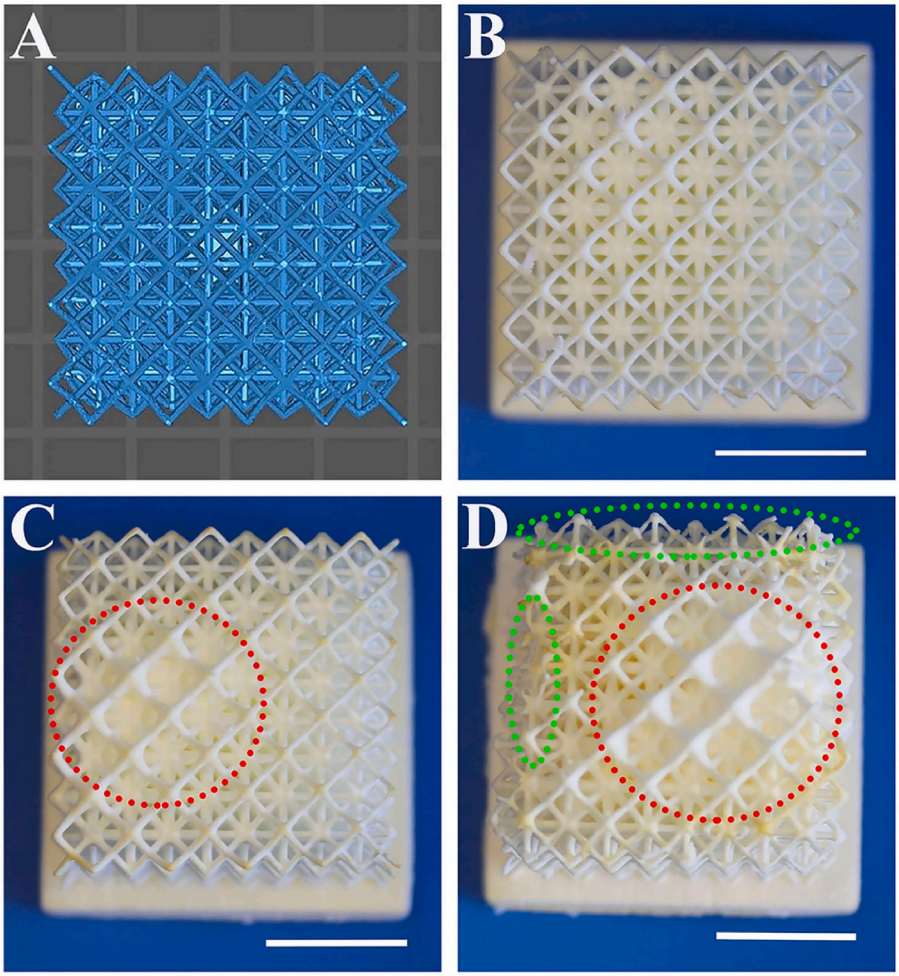

Fig. 1. **(A)** 3D design of tetrahedral octahedral vertex centroid lattice and digital images of 3D-printed polyHIPE lattices from **(B)** 80 % inherently porous HIPEs, **(C)** 85 % inherently porous HIPEs, and **(D)** 87.5 % inherently porous HIPEs from top view. Scale bars are 10 mm in all images. (A colour version of this figure can be viewed online.)

and data normalization was applied to the spectra in Origin Pro 2023. Additionally, polyHIPE samples were also examined as controls.

2.3.4. X-ray diffractometer (XRD)

The 85 % porous carboHIPE samples were analyzed by XRD using a PANalytical Aeris, operating at the 10 min scan measurement method (Cu tube 30 kV 40 mA, ¼° divergence slit, a 0.15 mm Ni filter, 0.02 Rad soller slits). The measurements were taken over at diffraction angles (2θs) from 0° to 100° with a step size of 0.02°.

2.3.5. Mechanical testing

Compression testing was performed to evaluate the mechanical properties of the 80 %, 85 %, and 87.5 % porous carboHIPE lattice structures fabricated at 800 °C (n = 4). A Mecmesin Multitest 2.5-dV mechanical testing machine equipped with a 250 N load cell was used at a rate of 1 mm/min. The data were collected using Vector Pro software.

2.3.6. Statistical analysis

Statistical analysis was conducted using Origin Pro 2023. To determine means, standard deviations, and significant differences, one-way ANOVA with Tukey's multiple comparison analysis was employed. Differences were considered significant when the p-value was less than or equal to 0.05. The specific number of replicates used in this study can be found in both the Materials and Methods section and the figure legend.

3. Results and discussion

3.1. Examination of the macro- and microstructure of inherently porous carboHIPE lattices

Before presenting the results of porous carboHIPE lattices, it is essential to examine the relationship between the internal phase ratio and 3D printing resolution. This understanding is crucial for accurately interpreting the structural changes that occur during pyrolysis, as the internal phase ratio has a direct impact on 3D printing resolution based on our findings.

3D-printed inherently porous polyHIPE lattice structures from their top view were presented in Fig. 1. Samples were named based on their nominal porosity (80 %, 85 %, and 87.5 %), which is the amount of internal phase used while preparing HIPEs to prevent confusion,

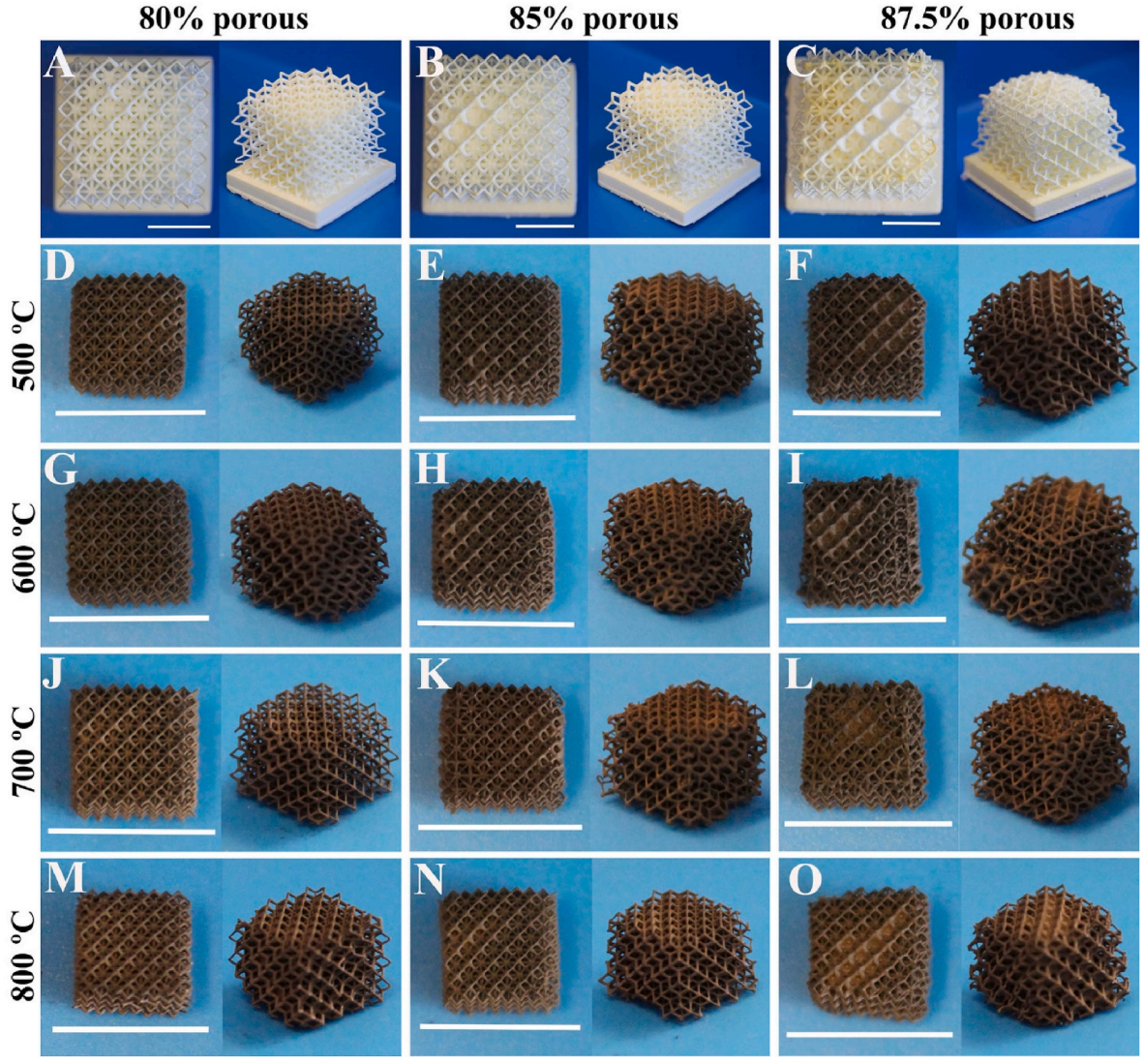

Fig. 2. Digital images of the 3D-printed polyHIPE and carboHIPE lattices from various perspectives. 80 % inherently porous **(A)** polyHIPE lattices and carboHIPE lattices pyrolyzed at **(D)** 500 °C, **(G)** 600 °C, **(J)** 700 °C, and **(M)** 800 °C. 85 % inherently porous **(B)** polyHIPE lattices and carboHIPE lattices pyrolyzed at **(E)** 500 °C, **(H)** 600 °C, **(K)** 700 °C, and **(N)** 800 °C. 87.5 % inherently porous **(C)** polyHIPE and carboHIPE lattices pyrolyzed at **(F)** 500 °C, **(I)** 600 °C, **(L)** 700 °C, and **(O)** 800 °C. Scale bars are 10 mm in all images. (A colour version of this figure can be viewed online.)

although it is different from their measured porosity. Fig. 1 exhibited the comparison in 3D printing resolution based on changing internal phase ratio.

The 80 % porous polyHIPEs feature a 1:4 ratio of external to internal phase, which is the optimum amount to 3D print lattice structures without overcuring. In our previous research, it was successfully demonstrated that the cubic vertex centroid lattice structure could be 3D printed without encountering overcuring issues by employing 80 % porous HIPEs [52]. The 85 % porous polyHIPEs employ a 1:5.67 ratio of external to internal phase while 87.5 % porous polyHIPEs have 1:7 ratio of external to internal phase. Some instances of overcuring were noted in the 85 % and 87.5 % porous 3D-printed polyHIPEs as marked with red circles in Fig. 1C–D. In addition to this, incomplete curing was observed in 87.5 % porous polyHIPEs, highlighted as green circles in Fig. 1D. This is due to the phase separation between the continuous phase and the internal phase during 3D printing. Based on these findings, as the internal phase ratio increased, the printing resolution decreased due to overcuring and/or incomplete curing, as illustrated in Fig. 1B–D.

3D-printed inherently porous polyHIPE lattice structures and their respective carboHIPE versions, subjected to various carbonization temperatures, specifically 500 °C, 600 °C, 700 °C, and 800 °C were presented in Fig. 2. These images provide visual representation and serve as a basis for the examination of these materials as the macrostructure is one of the main focuses of this study. This comprehensive collection of images, labeled from Fig. 2D–O, provides insight into the alterations of the hierarchically porous lattice structures resulting from different carbonization temperatures while Fig. 2A–C demonstrates inherently porous lattice structures with 80 %, 85 %, and 87.5 % porosity.

In addition to the visual inspection of shrinkage, the quantified data calculated shrinkage rates are presented in Table 1. The data in this table supplements the images in Fig. 2, providing a deeper insight into how the material behaves and changes during pyrolysis.

The volumetric shrinkage in all examined conditions is approximately 97 %. Interestingly, despite this significant shrinkage, the macrostructure was retained during isotropic contraction, preserving the integrity of the 3D strut network. Neither the degree of porosity nor the pyrolysis temperature exhibited a difference in the shrinkage behavior. Based on their standard deviations, a remarkable consistency in the shrinkage process is observed in all experimental conditions. Furthermore, the strut shrinkage within the lattices was measured at approximately 70 %, whereas the pore shrinkage was observed to be around 50 %. This disparity likely arises from the overall volume shrinkage being influenced by the combined contributions of both struts and pores. While the substantial reduction in strut dimensions contributes significantly to material shrinkage, the porosity remains relatively unchanged, with the pores exhibiting a less pronounced decrease in size. The observed volumetric shrinkage can be predominantly attributed to the cumulative reduction in strut thickness and density across the lattice structure, which exerts a more substantial influence on the total volume. The reduction of strut thickness is a convolution of densification during carbonization in combination with material evaporation.

A significant volumetric shrinkage (>80 %) is typically expected when carboHIPEs are derived from bare polyHIPEs. Researchers have successfully reduced this shrinkage to approximately 50 % using various strategies, including hyper-cross-linking [8,32], employing Pickering-stabilized HIPEs [34,35], sulfonation [59], porogen incorporation [60], and PEDOT-coating [40]. On the other hand, achieving such micro-sizes directly in the final shape is particularly challenging, especially for hierarchically porous carbon lattice structures. Therefore, the shrinkage can be advantageous for producing hierarchically porous microlattice carbon structures.

Figs. 3 and 4 presented SEM images of all carboHIPE lattices at various magnifications. These SEM images confirmed the observations from digital images concerning printing resolution. Overcured regions, indicated by red circles, are evident in the 85 % and 87.5 % porous carboHIPEs (Fig. 3), while no overcuring is observed in the 80 % porous carboHIPEs. Additionally, some distortion was noted in the 85 % and 87.5 % porous carboHIPEs at all pyrolysis temperatures (Fig. 4), identified by the bent appearance of the struts. A higher internal phase ratio resulted in regions of carboHIPEs that are not sufficiently robust to support their own weight. In contrast, the optimal internal phase ratio of 80 % did not exhibit such distortions.

The pore sizes determined by analyzing SEM images measure 21.20 ± 6.11 μm, 26.26 ± 7.33 μm, and 34.63 ± 13.15 μm in 80 %, 85 %, 87.5 % porous polyHIPEs. Higher porosity polyHIPEs exhibited larger pores. The mean pore sizes of carboHIPEs range between 11.66 and 16.63 μm, with more porous samples exhibiting more shrinkage of the pores. The pore size distributions, plotted against relative frequency (%), and their Gaussian fits were presented in the Supporting Information (Figs. S4, S6, S8, and S10). According to these analyses, polyHIPE samples exhibited pronounced positive skewness, indicating dominance of smaller pores, while 80 % and 85 % porous carboHIPEs showed a mix of skewed and balanced distributions at different temperatures. In contrast, 87.5 % porous carboHIPEs had more symmetric distributions at all temperatures.

Additionally, the degree of porosity stands at 64.02 % in 80 % porous polyHIPEs, 76.96 % in 85 % porous polyHIPEs, and 65.92 % in 87.5 % porous polyHIPEs. Interestingly, a notable difference exists between nominal porosity and measured porosity, which can be attributed to the decreasing stability of HIPEs during the 3D printing process [53]. On the other hand, the porosity of the carboHIPEs is between 59.13 and 75.09 % in 80 % porous carboHIPEs, 59.89 and 79.43 % in 85 % porous carboHIPEs and 55.38 and 73.48 % in 87.5 % porous carboHIPEs.

Table 1
Porosity (%), Density (g/cm^3), Shrinkage (vol. %), and Pore size (μm) values of the 80 %, 85 %, and 87.5 % porous polyHIPE lattices and carboHIPE lattices fabricated at 500 °C, 600 °C, 700 °C, and 800 °C.

Samples		Porosity (%)	Bulk density (g/cm^3)	Shrinkage (vol. %)	Pore size (μm)	Char yield (%)
80 % porous	**polyHIPE**	64.02	0.36	n/a	21.20 ± 6.11	n/a
	500°C	75.09	0.48	97.19 ± 0.10	15.12 ± 5.12	4.56
	600°C	59.13	0.41	97.39 ± 0.06	15.24 ± 5.14	4.98
	700°C	70.59	0.34	97.60 ± 0.03	16.63 ± 5.56	5.50
	800°C	68.61	0.19	97.47 ± 0.04	14.47 ± 4.50	5.54
85 % porous	**polyHIPE**	76.96	0.22	n/a	26.26 ± 7.33	n/a
	500°C	59.89	0.35	97.44 ± 0.04	14.66 ± 5.06	4.37
	600°C	74.45	0.25	97.39 ± 0.07	13.91 ± 4.56	3.02
	700°C	64.09	0.26	97.54 ± 0.02	12.49 ± 3.56	3.39
	800°C	79.43	0.14	97.70 ± 0.03	13.12 ± 3.65	4.35
87.5 % porous	**polyHIPE**	65.92	0.17	n/a	34.63 ± 13.15	n/a
	500°C	55.38	0.22	97.37 ± 0.08	13.04 ± 3.27	6.05
	600°C	73.48	0.24	97.19 ± 0.09	12.07 ± 2.98	4.62
	700°C	69.98	0.25	97.69 ± 0.01	12.21 ± 3.40	4.84
	800°C	71.04	0.14	97.19 ± 0.03	11.66 ± 2.82	6.05

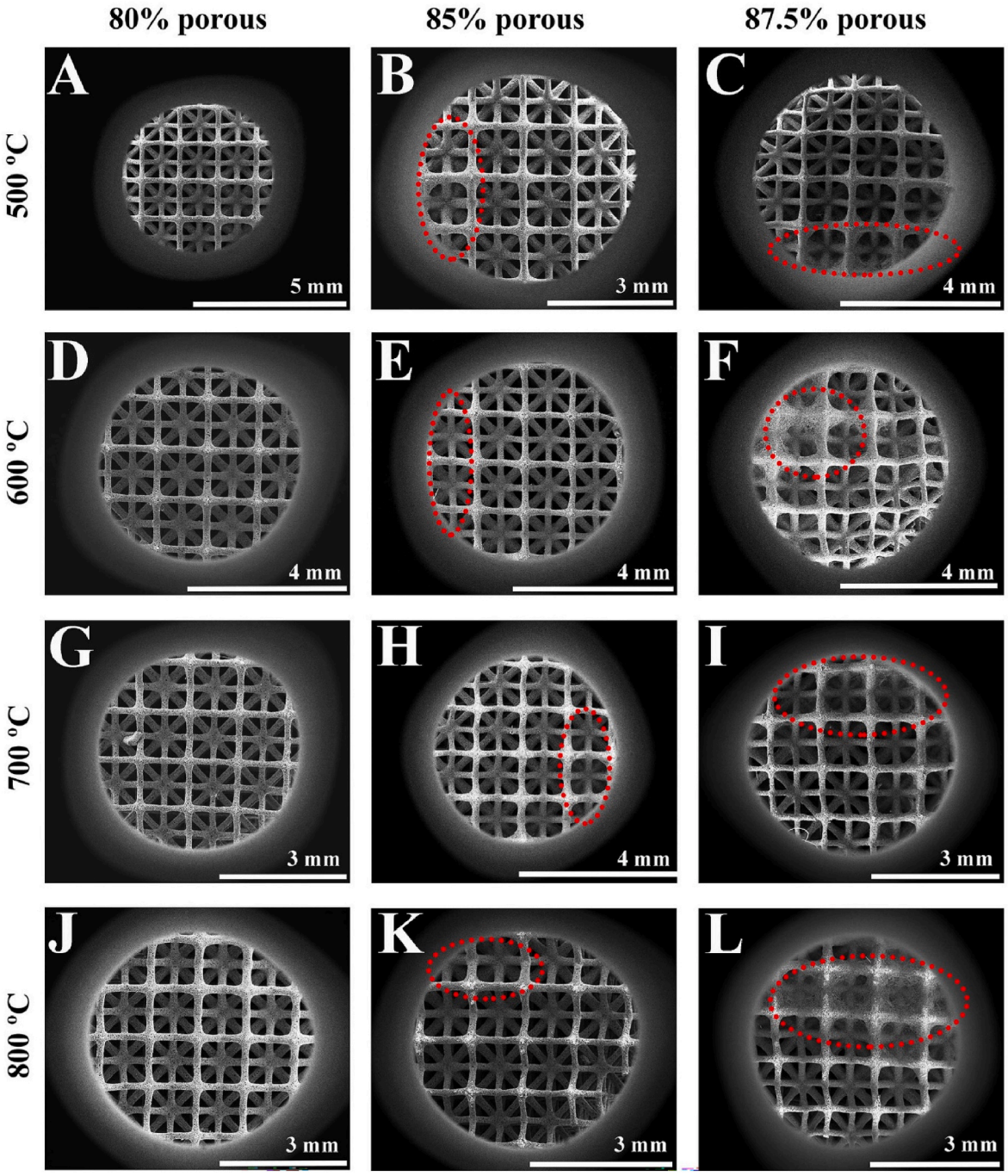

Fig. 3. SEM images of carboHIPE lattices. 80 % inherently porous carboHIPE lattices pyrolyzed at **(A)** 500 °C, **(D)** 600 °C, **(G)** 700 °C, and **(J)** 800 °C. 85 % inherently porous carboHIPE lattices pyrolyzed at **(B)** 500 °C, **(E)** 600 °C, **(H)** 700 °C, and **(K)** 800 °C. 87.5 % inherently porous carboHIPE lattices pyrolyzed at **(C)** 500 °C, **(F)** 600 °C, **(I)** 700 °C, and **(L)** 800 °C. (A colour version of this figure can be viewed online.)

Furthermore, there is no significant difference in porosity between polyHIPEs and carboHIPEs, indicating that porosity remains consistent throughout the pyrolysis process. In addition, bulk densities of polyHIPEs and carboHIPEs range from 0.14 to 0.48 g cm^{-3}. While there is no direct correlation between density and pyrolysis temperature, it is noteworthy that the highest temperature resulted in the lowest density. As expected, a higher degree of porosity led to lower density, as indicated in Table 1. The carboHIPE lattice structures developed in this study exhibit a highly porous architecture and low density. When compared to other very low-density carbonaceous materials, pyrolytic carbon lattices are typically fabricated at densities ranging from 0.6 to 1.4 g cm^{-3} [61–63]. In contrast, the inherently porous carboHIPEs demonstrated densities in the range of approximately 0.15–0.6 g cm^{-3} [34,40,42]. This comparison highlights that the carboHIPE lattice structures produced in this study reflect the typical density characteristics observed in carboHIPEs while being lighter than nonporous pyrolytic carbon lattices, as expected. In addition, the char yield of polyHIPEs ranges from 3 % to 6 %, which aligns with the TGA data (~11 %–2 % from 500 °C to 800 °C, respectively).

Although N_2 sorption analysis was not performed due to sample quantity limitations to measure specific surface area, previous studies on ST-co-DVB-based polyHIPEs suggest that the specific surface area significantly increases after pyrolysis, reaching approximately 500 m^2/g or higher [34,35,42].

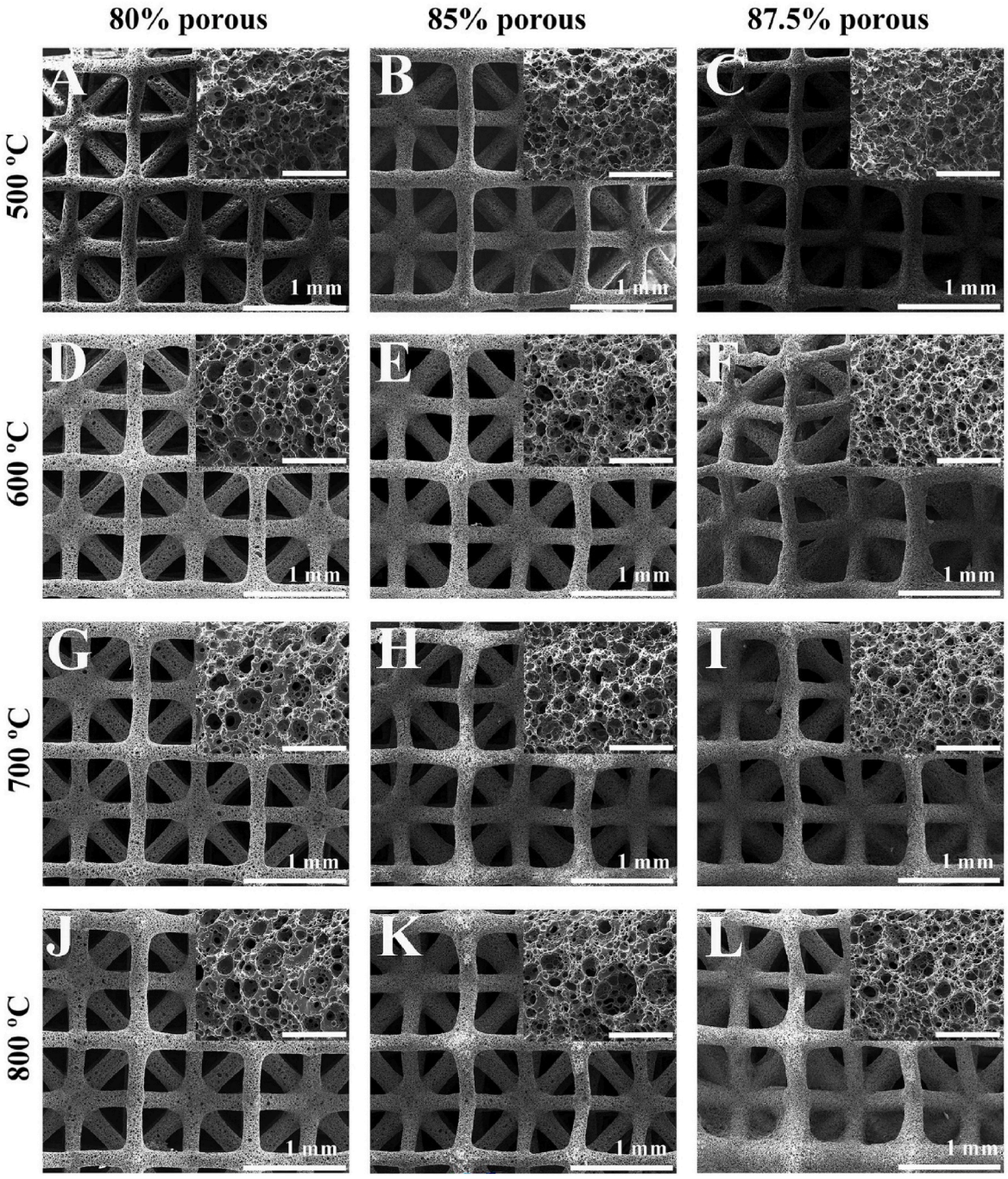

Fig. 4. SEM images of carboHIPE lattices at various magnifications. 80 % inherently porous carboHIPE lattices pyrolyzed at **(A)** 500 °C, **(D)** 600 °C, **(G)** 700 °C, and **(J)** 800 °C. 85 % inherently porous carboHIPE lattices pyrolyzed at **(B)** 500 °C, **(E)** 600 °C, **(H)** 700 °C, and **(K)** 800 °C. 87.5 % inherently porous carboHIPE lattices pyrolyzed at **(C)** 500 °C, **(F)** 600 °C, **(I)** 700 °C, and **(L)** 800 °C. Scale bars are 50 μm in all the insets. (A colour version of this figure can be viewed online.)

3.2. Carbonization mechanism of acrylate-based polyHIPEs

To investigate the degree of graphitization of carboHIPEs, Raman spectra were collected, and the corresponding data for 80 %, 85 %, and 87 % porous carboHIPEs were presented in Fig. 5A, B, and C, respectively. All samples demonstrated characteristic D and G bands at ~1349 cm^{-1} and ~1599 cm^{-1}, respectively. These peaks are indicative of the production of pyrolytic carbon and indicate the degree of carbonization (Fig. S7). The G band arises from the stretching vibrations of sp^2 carbon atoms whereas the D band is associated with the breathing modes of sp^2 carbon atoms in rings or chains, and its presence indicates structural defects or disorders [64]. Moreover, to calculate the D/G ratio, we used the relative height values of the peaks, determined from the normalized data. It was observed that, with the increase in the pyrolysis temperature, the intensity ratio of D to G exhibited an increase across all three distinct porosities (from ~0.6 to ~0.80). Furthermore, as anticipated, although porosity did not have a significant influence on these observed trends, the most highly porous samples displayed the lowest D/G ratios. To validate the carbon structure, XRD was conducted on 85 % porous carboHIPE samples manufactured at 500 °C, 600 °C, 700 °C, and 800 °C. The corresponding data is illustrated in Fig. 5D. The obtained XRD pattern exhibits characteristic broad peaks at 24° and 44°, corresponding to the (002) and (100) diffraction modes of pyrolytic carbon, respectively [65]. In addition, the difference in the peak positions

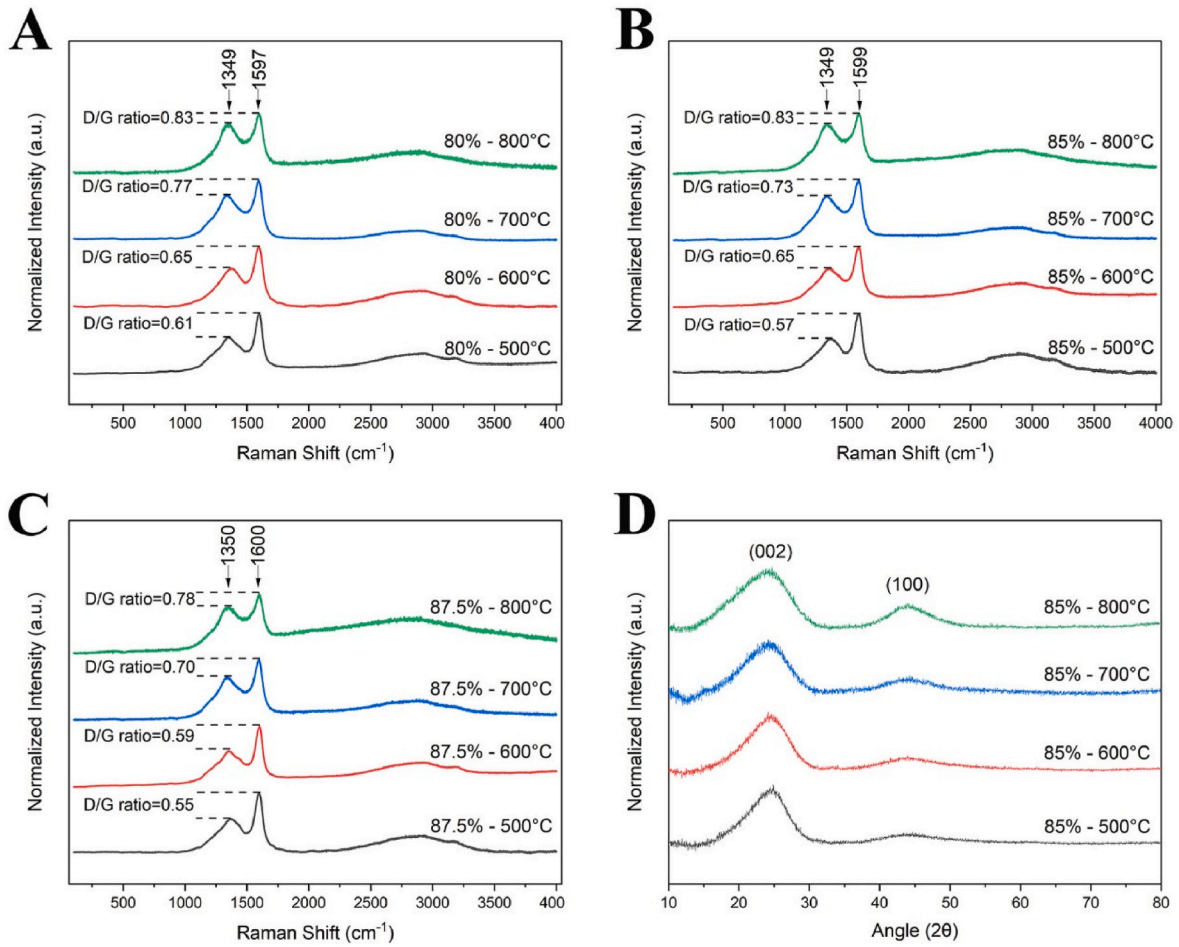

Fig. 5. Raman spectra of **(A)** 80 %, **(B)** 85 %, and **(C)** 87.5 % porous carboHIPEs and **(D)** XRD analysis of 85 % porous carboHIPEs fabricated at 500 °C, 600 °C, 700 °C, and 800 °C. (A colour version of this figure can be viewed online.)

compared to those of polyHIPE serves as evidence of successful carbonization (Fig. S7).

3.3. Mechanical properties of carboHIPEs

The final analysis aimed to assess the mechanical properties of carboHIPEs. Lattices with 80 %, 85 %, and 87.5 % porous configurations were fabricated at 800 °C for an investigation of their compressive mechanical properties.

The stress-strain curve of all samples (4 replicates in each category) and their representative comparison with each other are presented in Fig. 6. All samples were taken to failure as exhibited in Fig. 6D.

As seen the compressive response shows several peaks and troughs in the resulting stress as the strain (displacement) is increased. This can be attributed to regions of the material under a significant load which then reaches the failure point. This region of material will fail under the localized load, temporarily reducing the stress in the system as it redistributes. As the strain rises, the stress increases to a different region of the material, which then repeats until the material can no longer support any loads and eventually fails completely. Due to this process, the materials elastic moduli (Young's modulus) were determined by fitting the gradient up to the first peak [66].

The Balshin model [67], has primarily been used to describe strength reduction in metals and cements due to porosity and states

$$\sigma = \sigma_0(1-P)^a$$

Where σ is the compressive strength of the solid material and σ is the reduced strength due to porosity P. The factor of a is an empirical constant above 1. This shows that as the porosity rises, the strength of the material will decrease quickly, reducing the failure of the resulting internal structure.

Results of the samples show that the 85 % porous lattices exhibited the highest Young's modulus (1.28 ± 0.43 MPa). Furthermore, the 85 % and 87.5 % porous structures also exhibited fewer peaks in their compressive data compared to 80 % porous lattices.

To the best of our knowledge, previous production of carboHIPEs, carbon foams, and porous carbons has been limited to basic shapes [8,32,34,40] such as cubic or cylindrical forms, or carbon lattice structures fabricated from non-porous polymers [68,69] or fibers [70]. This study presents a novel approach where hierarchically porous carboHIPE lattice structures are fabricated for the first time by combining emulsion templating and vat photopolymerization, followed by pyrolysis.

4. Conclusions

In conclusion, this study systematically investigated the use of HIPEs with various porosities (80 %, 85 %, and 87.5 %) as 3D printing resins to fabricate inherently porous polyHIPE lattice structures and followed by the examination of macro- and microstructure, shrinkage behavior, pore characteristics, carbonization mechanisms, and mechanical properties of 3D-printed hierarchically porous carboHIPE lattices. While polyHIPEs with 85 % and 87.5 % porosity exhibited some overcured regions, the 87.5 % porous polyHIPEs also showed areas of incomplete curing. The examination of lattice structures at different carbonization temperatures showed consistent volumetric isotropic contraction. However, some

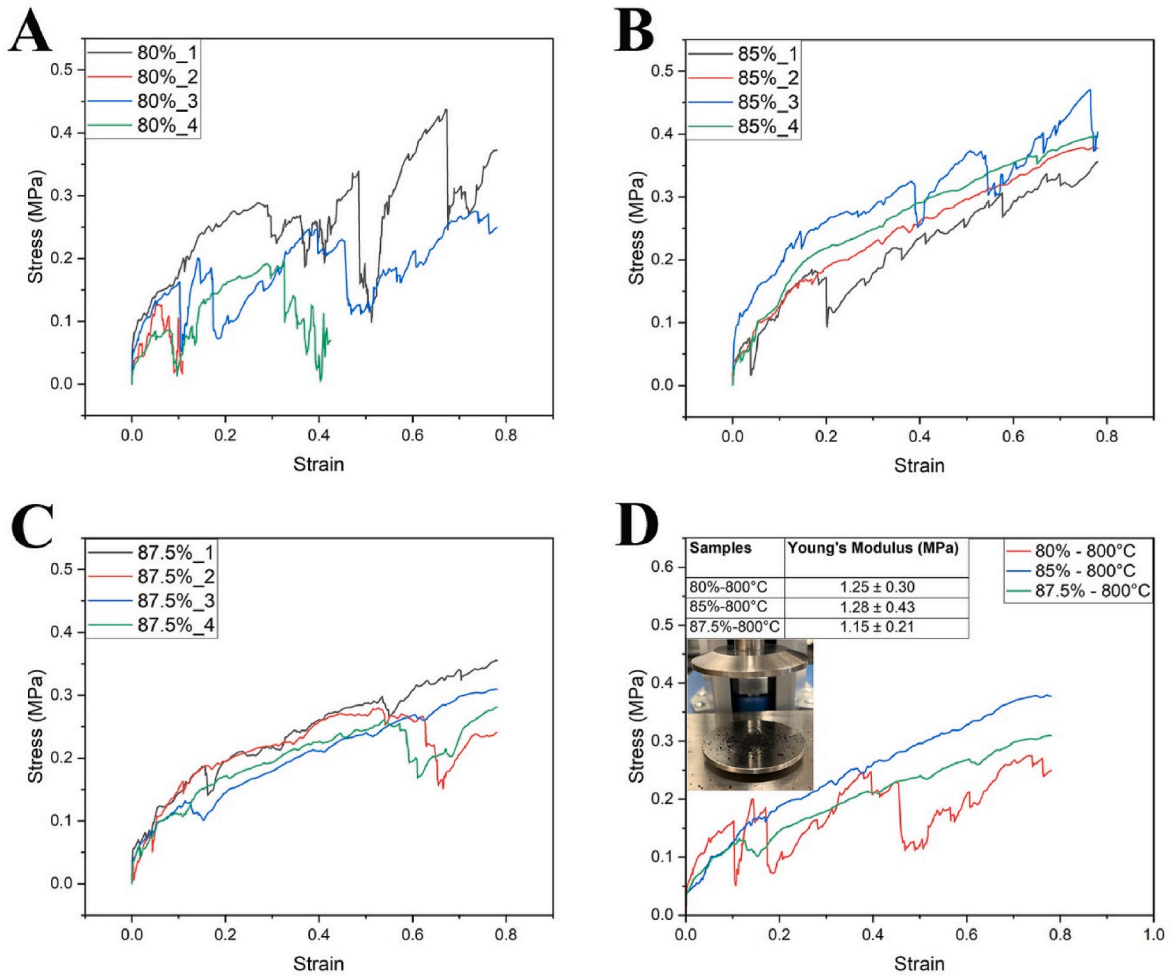

Fig. 6. Compression testing results of **(A)** 80 %, **(B)** 85 %, and **(C)** 87.5 % porous carboHIPE lattices pyrolyzed at 800 °C (n = 4) and **(D)** their representative comparison with each other. (A colour version of this figure can be viewed online.)

distortions were observed in 85 % and 87.5 % porous carboHIPEs due to the high internal phase content, with external to internal phase ratios of 1:5.67 and 1:7, respectively. Quantified data on shrinkage rates complemented visual inspections, showing approximately 97 % volumetric shrinkage with remarkable consistency across all conditions. SEM images displayed well-defined structures with varying pore sizes. Raman spectra indicated successful carbonization, with increasing intensity ratios of D/G bands (from ~0.6 to ~0.80) with increasing carbonization temperatures.

CRediT authorship contribution statement

Nihan Sengokmen-Ozsoz: Writing – original draft, Visualization, Validation, Methodology, Investigation, Conceptualization. **Rebecca Boston:** Writing – review & editing. **Julian S. Dean:** Writing – review & editing. **Cornelia Rodenburg:** Writing – review & editing, Conceptualization. **Frederik Claeyssens:** Writing – review & editing, Supervision.

Declaration of competing interest

The authors declare that they have no known competing financial interests or personal relationships that could have appeared to influence the work reported in this paper.

Acknowledgments

The authors acknowledge the Republic of Turkey, the Ministry of National Education for funding N. Sengokmen-Ozsoz. C. Rodenburg was funded by EPSRC (EP /V012126/1). F. Claeyssens also thanks the Royal Society for funding a Royal Society Leverhulme Trust Senior Research Fellowship in 2022 (SRF\R1\221053). We also acknowledge the Engineering and Physical Sciences Research Council (Grant No. EP /I007695/1) and the Medical Research Council (Grant No. MR/ L012669/1) for funding the equipment used in this study. We also acknowledge Dr Oday Hussein for conducting density and porosity measurements.

Appendix A. Supplementary data

Supplementary data to this article can be found online at https://doi.org/10.1016/j.carbon.2024.119933.

References

[1] M.S. Silverstein, PolyHIPEs: recent advances in emulsion-templated porous polymers, Prog. Polym. Sci. 39 (2014) 199–234, https://doi.org/10.1016/J.PROGPOLYMSCI.2013.07.003.
[2] N.R. Cameron, High internal phase emulsion templating as a route to well-defined porous polymers, Polymer (Guildf). 46 (2005) 1439–1449, https://doi.org/10.1016/j.polymer.2004.11.097.
[3] K.J. Lissant, B.W. Peace, S.H. Wu, K.G. Mayhan, Structure of high-internal-phase-ratio emulsions, J. Colloid Interface Sci. 47 (1974) 416–423, https://doi.org/10.1016/0021-9797(74)90273-2.

[4] T.A. Schaedler, A.J. Jacobsen, A. Torrents, A.E. Sorensen, J. Lian, J.R. Greer, L. Valdevit, W.B. Carter, Ultralight metallic microlattices, Science 334 (2011) 962–965, https://doi.org/10.1126/science.1211649.
[5] M.S. Pham, C. Liu, I. Todd, J. Lertthanasarn, Damage-tolerant architected materials inspired by crystal microstructure, Nature 565 (2019) 305–311, https://doi.org/10.1038/s41586-018-0850-3.
[6] L.J. Gibson, M.F. Ashby, Cellular solids: structure and properties, Cell. Solids Struct. Prop (2014) 1–510, https://doi.org/10.1017/CBO9781139878326. Second Ed., second edition.
[7] Y. Zeng, X. Du, H. Yao, P. Li, P. Dong, J. Chen, An Nylon lattice structure with improved mechanical property and energy absorption capability, Composer Part C Open Access 8 (2022) 100285, https://doi.org/10.1016/j.jcomc.2022.100285.
[8] R.T. Woodward, A. Jobbe-Duval, S. Marchesini, D.B. Anthony, C. Petit, A. Bismarck, Hypercrosslinked polyHIPEs as precursors to designable, hierarchically porous carbon foams, Polymer 115 (2017) 146–153, https://doi.org/10.1016/J.POLYMER.2017.03.042.
[9] A.D. Roberts, X. Li, H. Zhang, Porous carbon spheres and monoliths: morphology control, pore size tuning and their applications as Li-ion battery anode materials, Chem. Soc. Rev. 43 (2014) 4341–4356, https://doi.org/10.1039/C4CS00071D.
[10] M. Inagaki, H. Konno, O. Tanaike, Carbon materials for electrochemical capacitors, J. Power Sources 195 (2010) 7880–7903, https://doi.org/10.1016/J.JPOWSOUR.2010.06.036.
[11] G. Crini, Non-conventional low-cost adsorbents for dye removal: a review, Bioresour. Technol. 97 (2006) 1061–1085, https://doi.org/10.1016/J.BIORTECH.2005.05.001.
[12] S. Babel, T.A. Kurniawan, Low-cost adsorbents for heavy metals uptake from contaminated water: a review, J. Hazard Mater. 97 (2003) 219–243, https://doi.org/10.1016/S0304-3894(02)00263-7.
[13] Y. Zhao, X. Liu, Y. Han, Microporous carbonaceous adsorbents for CO2 separation via selective adsorption, RSC Adv. 5 (2015) 30310–30330, https://doi.org/10.1039/C5RA00569H.
[14] M.A. Mudassir, S. Kousar, M. Ehsan, M. Usama, U. Sattar, M. Aleem, et al., Emulsion-derived porous carbon-based materials for energy and environmental applications, Renew. Sustain. Energy Rev. 185 (2023) 113594, https://doi.org/10.1016/j.rser.2023.113594.
[15] J. Wang, H. Kong, J. Zhang, Y. Hao, Z. Shao, F. Ciucci, Carbon-based electrocatalysts for sustainable energy applications, Prog. Mater. Sci. 116 (2021) 100717, https://doi.org/10.1016/J.PMATSCI.2020.100717.
[16] J. Lee, J. Kim, T. Hyeon, Recent progress in the synthesis of porous carbon materials, Adv. Mater. 18 (2006) 2073–2094, https://doi.org/10.1002/ADMA.200501576.
[17] N. Patel, K. Okabe, A. Oya, Designing carbon materials with unique shapes using polymer blending and coating techniques, Carbon 40 (2002) 315–320, https://doi.org/10.1016/S0008-6223(01)00101-4.
[18] J. Gao, N. Ma, J. Tian, C. Shen, L. Wang, P. Yu, Y. Chu, W. Liu, X. Tan, X. Li, Z. Yin, High performance of N, P co-doped metal-free carbon catalyst derived from ionic liquid for oxygen reduction reaction, J. Solid State Electrochem. 22 (2018) 519–525, https://doi.org/10.1007/S10008-017-3785-Y.
[19] M.M. Rahman, M.M. Alam, A.M. Asiri, M.R. Awual, Fabrication of 4-aminophenol sensor based on hydrothermally prepared ZnO/Yb 2 O 3 nanosheets, New J. Chem. 41 (2017) 9159–9169, https://doi.org/10.1039/C7NJ01623A.
[20] Z. Yan, Z. Peng, J.M. Tour, Chemical vapor deposition of graphene single crystals, Acc. Chem. Res. 47 (2014) 1327–1337, https://doi.org/10.1021/AR4003043.
[21] O.S.G.P. Soares, R.P. Rocha, A.G. Gonçalves, J.L. Figueiredo, J.J.M. Órfão, M.F. R. Pereira, Easy method to prepare N-doped carbon nanotubes by ball milling, Carbon 91 (2015) 114–121, https://doi.org/10.1016/J.CARBON.2015.04.050.
[22] R. Borgohain, J. Yang, J.P. Selegue, D.Y. Kim, Controlled synthesis, efficient purification, and electrochemical characterization of arc-discharge carbon nano-onions, Carbon 66 (2014) 272–284, https://doi.org/10.1016/J.CARBON.2013.09.001.
[23] S. Joseph, G. Saianand, M.R. Benzigar, K. Ramadass, G. Singh, A.I. Gopalan, et al., Recent advances in functionalized nanoporous carbons derived from waste resources and their applications in energy and environment, Adv. Sustain. Syst. 5 (2021) 2000169, https://doi.org/10.1002/ADSU.202000169.
[24] M.A. Mudassir, H.Z. Aslam, T.M. Ansari, H. Zhang, I. Hussain, Fundamentals and design-led synthesis of emulsion-templated porous materials for environmental applications, Adv. Sci. 8 (2021) 2102540, https://doi.org/10.1002/ADVS.202102540.
[25] B. Aldemir Dikici, F. Claeyssens, Basic principles of emulsion templating and its use as an emerging manufacturing method of tissue engineering scaffolds, Front. Bioeng. Biotechnol. 8 (2020) 875, https://doi.org/10.3389/FBIOE.2020.00875.
[26] B. Aldemir Dikici, S. Dikici, F. Claeyssens, Synergistic effect of type and concentration of surfactant and diluting solvent on the morphology of emulsion templated matrices developed as tissue engineering scaffolds, React. Funct. Polym. 180 (2022) 105387, https://doi.org/10.1016/J.REACTFUNCTPOLYM.2022.105387.
[27] A. Menner, V. Ikem, M. Salgueiro, M.S.P. Shaffer, A. Bismarck, High internal phase emulsion templates solely stabilised by functionalised titania nanoparticles, Chem. Commun. 41 (2007) 4274–4276, https://doi.org/10.1039/B708935J.
[28] E. Durgut, C. Sherborne, B. Aldemir Dikici, G.C. Reilly, F. Claeyssens, Preparation of interconnected pickering polymerized high internal phase emulsions by arrested coalescence, Langmuir 38 (2022) 10953–10962, https://doi.org/10.1021/acs.langmuir.2c01243.
[29] E. Durgut, M. Zhou, B.A. Dikici, R. Foudazi, F. Claeyssens, Modifying pickering polymerized high internal phase emulsion morphology by adjusting particle hydrophilicity, Colloids Surfaces A Physicochem. Eng. Asp. 680 (2023) 132629, https://doi.org/10.1016/J.COLSURFA.2023.132629.
[30] R. Foudazi, HIPEs to polyHIPEs, React. Funct. Polym. 164 (2021) 104917, https://doi.org/10.1016/J.REACTFUNCTPOLYM.2021.104917.
[31] D. Wang, Preparation, Properties and Applications of Highly Porous Polymer, Carbon, and Silica-Carbon Monoliths Derived from High Internal Phase Emulsions, The University of Manhester, 2004.
[32] S. Israel, I. Gurevitch, M.S. Silverstein, Carbons with a hierarchical porous structure through the pyrolysis of hypercrosslinked emulsion-templated polymers, Polymer 72 (2015) 453–463, https://doi.org/10.1016/J.POLYMER.2015.02.055.
[33] D. Wang, N.L. Smith, P.M. Budd, Polymerization and carbonization of high internal phase emulsions, Polym. Int. 54 (2005) 297–303, https://doi.org/10.1002/PI.1672.
[34] R.T. Woodward, D.W.H. Fam, D.B. Anthony, J. Hong, T.O. McDonald, C. Petit, M.S. P. Shaffer, A. Bismarck, Hierarchically porous carbon foams from pickering high internal phase emulsions, Carbon 101 (2016) 253–260, https://doi.org/10.1016/j.carbon.2016.02.002.
[35] R.T. Woodward, F. De Luca, A.D. Roberts, A. Bismarck, High-surface-area, emulsion-templated carbon foams by activation of polyHIPEs derived from pickering emulsions, Materials 9 (9) (2016) 776, https://doi.org/10.3390/MA9090776.
[36] S. Ungureanu, G. Sigaud, G.L. Vignoles, C. Lorrette, M. Birot, H. Deleuze, R. Backov, First biosourced monolithic macroporous SiC/C composite foams (bio-SiC/C(HIPE)) bearing unprecedented heat transport properties, Adv. Eng. Mater. 15 (2013) 893–902, https://doi.org/10.1002/ADEM.201300015.
[37] N. Cohen, M.S. Silverstein, Synthesis of emulsion-templated porous polyacrylonitrile and its pyrolysis to porous carbon monoliths, Polymer 52 (2011) 282–287, https://doi.org/10.1016/J.POLYMER.2010.11.026.
[38] M. Liu, L. Gan, F. Zhao, H. Xu, X. Fan, C. Tian, X. Wang, Z. Xu, Z. Hao, L. Chen, Carbon foams prepared by an oil-in-water emulsion method, Carbon 45 (2007) 2710–2712, https://doi.org/10.1016/J.CARBON.2007.08.004.
[39] A. Szczurek, V. Fierro, A. Pizzi, A. Celzard, Emulsion-templated porous carbon monoliths derived from tannins, Carbon 74 (2014) 352–362, https://doi.org/10.1016/J.CARBON.2014.03.047.
[40] A. Suresh, S.J. Rowan, C. Liu, Macroscale fabrication of lightweight and strong porous carbon foams through template-coating pair design, Adv. Mater. 35 (2023), https://doi.org/10.1002/adma.202206416.
[41] R. Woodward, F. Markoulidis, D.W.H. Fam, T.O. Mcdonald, F. De Luca, M.S. P. Shaffer, A. Bismarck, Carbon foams from polyhipe/reduced graphene oxide composites and their performance as electrodes, in: Supercapacitor Devices, AIChE Annual Meeting, 2016.
[42] R.T. Woodward, F. Markoulidis, F. De Luca, D.B. Anthony, D. Malko, T. O. McDonald, M.S.P. Shaffer, A. Bismarck, Carbon foams from emulsion-templated reduced graphene oxide polymer composites: electrodes for supercapacitor devices, J. Mater. Chem. A 6 (2018) 1840–1849, https://doi.org/10.1039/C7TA09893F.
[43] H.D. Asfaw, R. Younesi, M. Valvo, J. Maibach, J. Ångström, C.W. Tai, Z. Bacsik, M. Sahlberg, L. Nyholm, P.K. Edström, Boosting the thermal stability of emulsion–templated polymers via sulfonation: an efficient synthetic route to hierarchically porous carbon foams, ChemistrySelect 1 (2016) 784–792, https://doi.org/10.1002/SLCT.201600139.
[44] Y. Kawai, T. Yamamoto, Synthesis of porous carbon hollow particles maintaining their structure using hyper-cross-linked Poly(St-DVB) hollow particles, Adv. Powder Technol. 31 (2020) 614–620, https://doi.org/10.1016/J.APT.2019.11.016.
[45] Z. Wang, D. Cheng, C. Chen, K. Zhou, Hierarchically porous carbon microspheres with fully open and interconnected super-macropores for air cathodes of Zn-Air batteries, Carbon N. Y. 136 (2018) 54–62, https://doi.org/10.1016/J.CARBON.2018.04.061.
[46] H.D. Asfaw, M. Roberts, R. Younesi, K. Edström, Emulsion-templated bicontinuous carbon network electrodes for use in 3D microstructured batteries, J. Mater. Chem. A 1 (2013) 13750–13758, https://doi.org/10.1039/C3TA12680C.
[47] N. Díez, M. Sevilla, A.B. Fuertes, Synthesis strategies of templated porous carbons beyond the silica nanocasting technique, Carbon 178 (2021) 451–476, https://doi.org/10.1016/J.CARBON.2021.03.029.
[48] S. Kovačič, B. Schafzahl, N.B. Matsko, K. Gruber, M. Schmuck, S. Koller, et al., Carbon foams via ring-opening metathesis polymerization of emulsion templates: a facile method to make carbon current collectors for battery applications, ACS Appl. Energy Mater. 5 (2022) 14381–14390, https://doi.org/10.1021/ACSAEM.2C02787.
[49] S. Kovačič, K. Gruber, B. Fuchsbichler, M. Schmuck, C. Slugovc, Macroporous carbon coatings through carbonization of emulsion-templated poly (dicyclopentadiene) on metal substrates, Monatshefte Fur Chemie 154 (2023) 515–522, https://doi.org/10.1007/S00706-023-03048-5.
[50] D.W. Johnson, C. Sherborne, M.P. Didsbury, C. Pateman, N.R. Cameron, F. Claeyssens, Macrostructuring of emulsion-templated porous polymers by 3D laser patterning, Adv. Mater. 25 (2013) 3178–3181, https://doi.org/10.1002/adma.201300552.
[51] R. Owen, C. Sherborne, T. Paterson, N.H. Green, G.C. Reilly, F. Claeyssens, Emulsion templated scaffolds with tunable mechanical properties for bone tissue engineering, J. Mech. Behav. Biomed. Mater. 54 (2016) 159–172, https://doi.org/10.1016/j.jmbbm.2015.09.019.
[52] C. Sherborne, R. Owen, G.C. Reilly, F. Claeyssens, Light-based additive manufacturing of PolyHIPEs: controlling the surface porosity for 3D cell culture applications, Mater. Des. 156 (2018) 494–503, https://doi.org/10.1016/j.matdes.2018.06.061.

[53] N. Sengokmen Ozsoz, S. Pashneh-Tala, F. Claeyssens, Optimization of a high internal phase emulsion-based resin for use in commercial vat photopolymerization additive manufacturing, 3D print, Addit. Manuf. 11 (2) (2024) 496–507, https://doi.org/10.1089/3DP.2022.0235.
[54] N. Sengokmen-Ozsoz, R. Boston, F. Claeyssens, Investigating the potential of electroless nickel plating for fabricating ultra-porous metal-based lattice structures using PolyHIPE templates, ACS Appl. Mater. Interfaces 15 (2023) 30769–30779, https://doi.org/10.1021/ACSAMI.3C04637.
[55] S.J. Pierre, J.C. Thies, A. Dureault, N.R. Cameron, J.C.M. Van Hest, N. Carette, et al., Covalent enzyme immobilization onto photopolymerized highly porous monoliths, Adv. Mater. 18 (2006) 1822–1826, https://doi.org/10.1002/adma.200600293.
[56] Elegoo. https://www.elegoo.com/products/elegoo-saturn-2-8k-10-inches-mono-lcd-3d-printer. (Accessed 24 September 2024).
[57] A. Uhlemann, Lattice structures - mikrostrukturen. https://www.thingiverse.com/thing:2788117. (Accessed 24 September 2024).
[58] A. Barbetta, N.R. Cameron, Morphology and surface area of emulsion-derived (PolyHIPE) solid foams prepared with oil-phase soluble porogenic solvents: span 80 as surfactant, Macromolecules 37 (2004) 3188–3201, https://doi.org/10.1021/MA0359436.
[59] U.M. Patil, R. V Ghorpade, M. Sik Nam, A.C. Nalawade, S. Lee, H. Han, et al., PolyHIPE derived freestanding 3D carbon foam for cobalt hydroxide nanorods based high performance supercapacitor, Sci. Rep. 6 (1) (2016) 35490, https://doi.org/10.1038/srep35490.
[60] S. Israel, M. Levin, S. Oliel, D. Mayer, I. Lerner, M.S. Silverstein, Hierarchical porosity in emulsion-templated, porogen-containing interpenetrating polymer networks: hyper-cross-linking and carbonization, Macromolecules 55 (2022) 1992–2002, https://doi.org/10.1021/ACS.MACROMOL.1C01432.
[61] C.M. Portela, B.W. Edwards, D. Veysset, Y. Sun, K.A. Nelson, D.M. Kochmann, et al., Supersonic impact resilience of nanoarchitected carbon, Nat. Mater. 20 (2021) 1491–1497, https://doi.org/10.1038/s41563-021-01033-z.
[62] X. Zhang, A. Vyatskikh, H. Gao, J.R. Greer, X. Li, Lightweight, flaw-tolerant, and ultrastrong nanoarchitected carbon, Proc. Natl. Acad. Sci. U.S.A. 116 (2019) 6665–6672, https://doi.org/10.1073/PNAS.1817309116.
[63] X. Zhang, L. Zhong, A. Mateos, A. Kudo, A. Vyatskikh, H. Gao, et al., Theoretical strength and rubber-like behaviour in micro-sized pyrolytic carbon, Nat. Nanotechnol. 14 (2019) 762–769, https://doi.org/10.1038/s41565-019-0486-y.
[64] A.C. Ferrari, J. Robertson, Interpretation of Raman spectra of disordered and amorphous carbon, Phys. Rev. B 61 (20) (2000) 14095.
[65] Z.Q. Li, C.J. Lu, Z.P. Xia, Y. Zhou, Z. Luo, X-ray diffraction patterns of graphite and turbostratic carbon, Carbon 45 (2007) 1686–1695, https://doi.org/10.1016/J.CARBON.2007.03.038.
[66] Y. Chen, H. Liu, J. Shen, J. Gong, J. Zhao, Compression behavior of diamond lattice structure and its Hall–petch relationship, Adv. Eng. Mater. 23 (2021) 2001024, https://doi.org/10.1002/ADEM.202001024.
[67] M.Y. Balshin, Relation of mechanical properties of powder metals and their porosity and the ultimateproperties of porous-metal ceramic materials, Dokl. Akad. Nauk SSSR 67 (1949) 831–834.
[68] A.J. Jacobsen, S. Mahoney, W.B. Carter, S. Nutt, Vitreous carbon micro-lattice structures, Carbon 49 (2011) 1025–1032, https://doi.org/10.1016/J.CARBON.2010.10.059.
[69] Y. Katsuyama, J. Hui, M. Thiel, N. Haba, Z. Yang, R.B. Kaner, 3D-Printed carbon scaffold for structural lithium metal batteries, Small Methods (2024) 2400831, https://doi.org/10.1002/smtd.202400831.
[70] H. McClintock, Z. Xiong, B. Rergis, H. Lipson, Design and fabrication of carbon fiber lattices using 3D weaving, Sci. Rep. 13 (1) (2023) 14919, https://doi.org/10.1038/s41598-023-40962-4.